CCFE
CULHAM CENTRE FOR FUSION ENERGY

UK Atomic Energy Authority

UKAEA-CCFE-PR(23)98

Francesco Palermo et al.

Modulation behaviour and existence criterion of geodesic acoustic modes

Modulation behaviour and existence criterion of geodesic acoustic modes

Francesco Palermo et al.

This is a preprint of a paper submitted for publication in
Nuclear Fusion

Modulation behaviour and possible existence criterion of geodesic acoustic modes in tokamak devices

F. Palermo,[1, a)] G. D. Conway,[2] E. Poli,[2] and C. M. Roach[1]
[1)] *Culham Science Centre, Abingdon, OX14 3DB, UK*
[2)] *Max-Planck-Institut für Plasmaphysik, Garching, Germany*

(Dated: 22 December 2022)

Geodesic acoustic modes (GAMs) represent the oscillating counterpart of zonal flow in tokamak plasma and can affect transport due to their interaction with turbulence eddies. GAMs have been observed in many experiments and modelled under different conditions, but because of their variety of characteristics, we do not yet have a complete picture of their dynamics. It has been demonstrated that optical methods can be efficiently used to describe and predict several characteristics of the GAM radial structures that can be interpreted as "waves" propagating in the space-time. We exploit eikonal and paraxial WKB theory to investigate the behaviour of GAMs that are commonly observed in experiments, and find that their periodic modulation and intermittency can be explained by the properties of the equilibrium temperature profile. Theoretical results obtained in this work are supported by gyrokinetic simulations for several equilibria. Implications for existence criteria and GAM dynamics in different plasma equilibrium conditions are discussed, with particular attention to the edge plasma in low and high confinement modes.

Keywords: Geodesic Acoustic Mode, dispersion, damping, intermittency

I. INTRODUCTION

At the edge of a tokamak device, drift waves and turbulence are influenced by the oscillating counterpart of zonal flows know as geodesic acoustic modes (GAMs). These modes are oscillations characterized by poloidal and toroidal $(m, n) = 0, 0$ wave number perturbations of the electrostatic potential coupled with pressure $(m, n) = 1, 0$ perturbations[1]. An exhaustive paper including current knowledge of GAMs has been recently published[2]. Because of their action on turbulence cells, it is believed that GAMs play an important role in establishing the level of turbulent transport.

In fact, their frequency typically around 20 kHz in present-day tokamaks is slow enough to radially shear turbulent eddies and reduce the associated cross-field transport. Their quasi-static character may make their action perhaps less effective than that of stationary zonal flows in turbulent transport reduction. However, GAMs provide an additional energy dissipation route for the turbulence via Landau and collisional damping. Thus, GAMs are expected to have an equivalent role to that of zonal flows in moderating edge turbulence behavior[3]. GAMs are thought to be non-linearly driven by turbulence and linearly damped by collisionless ion Landau damping in the typical range of parameters in which tokamak machines operate.

Studies of GAMs are the most flourishing area in zonal flow experiments. Many devices have provided information on the basic features of GAMs, such as their axisymmetric structure, dispersion relation, couplings with turbulence and accompanying density fluctuations (see Ref. 2 and references therein). So far, most observations show good agreement with predictions made using existing theories. For example, the essential dependence of the GAM frequency should obey the theoretical expectation. This has been confirmed in tokamaks, spherical tokamaks such as MAST[4,5] as well as stellarators. Although extensive efforts have been made over the last decades in zonal flow experiments, a number of issues remain to be explored. Moreover, this huge quantity of experimental results have revealed many interesting characteristics that are yet to be understood theoretically. For example, eigenmodes are often observed in experiments with frequencies that do not follow trends predicted from the temperature profile[4,6]; GAM frequency splitting are observed in ASDEX Upgrade (AUG) and DIIID[6,7]; GAMs separating into two parts that move in opposite directions[8]; and GAM modulation and/or intermittency in amplitude and frequency[2,5,9].

This last aspect is a common GAM characteristic observed in different conventional and spherical tokamak machines in steady plasma conditions. In fact, intermittent GAM behaviour is often observed around a clear spectral signal, that as mentioned previously, is typically around 20 kHz. Sometimes in steady state conditions it is possible to observe a modulation of the GAM frequency. This has been documented and investigated experimentally. The modulation appears to be different from zonal flow poloidal modulations whose causes can be found in shear flow instabilities such as Kelvin-Helmholtz[10–13]. GAM modulations can be more or less regular or can degenerate in a burst. We note that modulation in AUG appears to be more regular and sinusoidal compared to other machines such as T-10. The intermittency of GAMs has been quantified, revealing that the autocorrelation time ranges from about 5 to 20 GAM periods in cases examined, a difference that affects the probability distribution function of the $E \times B$ velocity at

[a)] Electronic mail: francesco.palermo@ukaea.uk

the GAM frequency. The frequency of this intermittent behavior generally varies between ~ 0.2 kHz and ~ 1 kHz and the physical reason for the modulation is not fully understood.

One candidate explanation has been proposed by considering a radial displacements of GAMs due to temperature fluctuations. However, no significant variations have been observed in the ECE diagnostic, nor in the plasma position data. A possible correlation with magnetic fluctuations observed at around 0.2 kHz has also been ruled out. The most plausible explanation seems to be a correlation between the GAM intensity and low frequency zonal flows, via Alfvén-drift wave turbulence[9,14]. Moreover, averaged bispectral analysis shows that the strength of the nonlinear interaction of the GAM with broadband turbulence can vary with the magnitude of the GAM. Thus, the modulation in the GAM amplitude and frequency appears related with the density fluctuation level[15]. In Tore Supra GAMs were modulated in amplitude and in frequency around 100 Hz. In T-10 the frequency of GAMs was several kHz. In HL-2A the modulation can be particularly strong.

Generally, when the GAM peak is reduced the broadband background spectrum is enhanced-suggesting an increase in the random E_r fluctuations [6]. This feature is very reproducible and is highly significant as it points towards the predicted interaction between GAM/ZF and the turbulence amplitude.

In this work we investigate aspects related to the oscillation and intermittency of GAMs by applying techniques derived from the field of optics. We have already shown how optical theories represent a robust basis for the description of many characteristics of radial propagation and spreading of GAMs[16–19,21]. Here we continue to investigate the GAM behaviour using these methods in order to describe analytically a certain number of observations and, where possible, to predict behavior. We study GAMs in the low confinement L-mode and at the L to H-mode transition, providing further insights with respect to Refs. 22 and 23 as to why GAMs are not observed experimentally in H-modes.

We recall that GAMs are universally observed in ohmic and heated L-mode regimes[24]. However, they have not to-date been seen in high power H-modes[9,25] (note contrary result from EAST).

There are several open issues: what happens to GAMs across the L-H transition?; what is the role of GAMs in the self-suppression of edge turbulence in H-mode or in triggering the transition through enhanced eddy shearing?; and what is the interaction between GAMs and the mean shear flow? We recall that strong GAMs are observed across the edge region in the L-mode phase, but their radial extent narrows as the discharge enters an intermediate improved confinement state (I-phase)[25]. As the H-mode transition approaches an increase in frequency and amplitude modulation of the GAMs is observed. This aspect is correlated with an increase of the broadband turbulent flow and density fluctuation modulation. Finally, when the H-mode regime is established, the density turbulence is quenched across the pedestal region, and the GAM disappears into the background fluctuation level. Some of these aspects will be investigated in the present paper.

The paper is organized as follows. In Sec. II we briefly recall the principal aspects of the code and normalizations used in our numerical model. Sec. III first discusses the theory adopted to describe GAMs with a particular focus on the effects of the second radial derivative of the temperature gradient. In Sec. IV we present the simulation results and compare these with analytical theory. After demonstrating the validity of the theory, we apply this to a range of parameters of interest derived from two different AUG shots in L- and H-mode, in which frequency modulation is observed and GAMs are not present respectively. Finally in Sec. VI we present the conclusion and the implications of this work.

II. NUMERICAL MODEL

The gyrokinetic ORB5 code used in this work has been extensively described previously and consequently we limit ourselves in this section to briefly recalling its principal characteristics[26]. The code uses a Lagrangian formulation based on the gyrokinetic (GK) Vlasov-Maxwell system of equations and now includes all extensions made in the NEMORB project[27,28]. The particle gyrocentre trajectories are computed from equations derived from the variational principles on the action. The code solves the full-f gyrokinetic Vlasov equation using a particle-in-cell δf method. The δf quantity represents the fluctuating part of the distribution function and is discretized using a population of numerical particles called markers. Energy and momentum conservations can be proven via gyrokinetic field theory[29]. To obtain the perturbed potential, the Vlasov equation must be coupled with equations for the fields. These are obtained by taking functional derivatives of the actions with respect the perturbed potential, leading to a polarization equation for ϕ and the Ampére law for $A_{||}$. In this work we have used the electrostatic version of the model with a single ion species and adiabatic electrons. The corresponding polarization equation reduces to the standard linear quasi-neutrality condition of Hahm[30], written in the long wave-length limit. ORB5 is massively parallelized. In the code, time t is normalized to the inverse of the ion cyclotron frequency $\Omega_i = eB_0/m_i$, the radial direction is normalized in terms of $\rho_s = \sqrt{k_B T_{e,0} m_i}/(eB_0)$ with $T_{e,0}$ the electron temperature, and the potential is given in $\phi_0 = k_B T_{e,0}/e$ units. We indicate $L_r = 2/\rho^*$ by denoting the magnetisation $1/\rho^* = a/\rho_s$, where a is the minor radius at the midplane. The quantity B_0 is calculated at the magnetic axis, while $T_{e,0}$ is calculated in the middle of the radial domain. The ion Larmor radius is defined as $\rho_i = \sqrt{2}\sqrt{T_{i,0}/T_{e,0}}\rho_s$ with $T_{i,0}$ the ion temperature, also calculated in the middle of the radial domain.

III. OPTICAL TREATMENT OF GAM DYNAMICS

Before introducing the new results from this work, in this section we briefly summarize findings from earlier studies of GAMS using optical theory. Geodesic acoustic modes are waves that, as mentioned in the introduction, are characterized by $(m, n = 0, 0)$ mode numbers for the electric field and can be considered in a first approximation to vary essentially along the radial direction. The GAM dispersion relation to second order in $k_r\rho_i$ can be written as[31,32]:

$$\omega = \omega_G\Big(1 + \frac{1}{2}\alpha_1 k_r^2\rho_i^2\Big) \tag{1}$$

where the frequency ω_G is a function of $\tau_e = T_i/T_e$ and of ion thermal velocity $v_{th,i}$ and major radius R_0:

$$\omega_G = \Big[1 + \frac{2(23 + 16\tau_e + 4\tau_e^2)}{q^2(7 + 4\tau_e)}\Big]^{1/2}\Big(\frac{7}{4} + \tau_e\Big)^{1/2}\frac{v_{th,i}}{R_0} \tag{2}$$

$$\alpha_1 = \frac{1}{2}\Big[\frac{3}{4} - \Big(\frac{7}{4} + \tau_e\Big)^{-1}\Big(\frac{13}{4} + 3\tau_e + \tau_e^2\Big) + (\frac{7}{4} + \tau_e)^{-2}\Big(\frac{747}{32} + \frac{481}{32}\tau_e + \frac{35}{8}\tau_e^2 + \frac{1}{2}\tau_e^3\Big)\Big] \tag{3}$$

We note that in Eq. 3, $\alpha_1 > 0$ for $\tau_e \lesssim 5.54$. In our treatment, we adopt Eqs. 2 and 3, neglecting effects related to plasma elongation, triangularity and so on, to focus on the essential aspect of the problem. As we have presented in Ref. 18 we can establish a certain parallel between light beam evolution in a medium and GAM dynamics that becomes evident on comparing the stationary two-dimensional Helmholtz equation:

$$(\nabla^2 + k_0^2 n_0^2)E = \Big[\frac{\partial}{\partial x^2} + \frac{\partial}{\partial y^2} + \bar{n}_0^2\Big]E = 0 \tag{4}$$

with the wave equation of GAMs:

$$\Big[+\frac{1}{\omega_G^2}\frac{\partial}{\partial t^2} - \alpha_1\rho_i^2\frac{\partial}{\partial r^2} + 1\Big]E = 0 \tag{5}$$

In this way, we observe that Eq.5 appears as the normalized version with $\bar{n}_0 = k_0 n_0 = 1$ of Eq. 4, with $x \to \omega_G t$ and $y \to r/\sqrt{\alpha_1}\rho_i$). This analogy allows us to describe the GAM evolution in terms of refraction, interference and diffraction effects in a medium with a certain associated index of refraction n_G in space-time. It is important to emphasize that the analogy between Eq. 4 and Eq. 5 is completely established for $\alpha_1 < 0$. In fact, for these α_1 values, characteristics of waves for which phase path and wave front trajectories are perpendicular each others are respected. However, the analogy between the two equations continues to be valid also for $\alpha_1 > 0$ by paying attention to the fact that a positive value of α_1 reverses the concavity of the wave front in the space-time plane (see Fig. 1 and Fig. 2 of Ref. 18). In our previous paper Ref. 18, we focused on the applicability of two different complex eikonal methods to describe the spreading of GAMs. As a result it has been possible to associate with GAMs an index of refraction as a function of the temperature profile via ω_G and ρ_i. The associated refractive index is a function of space and time and this, in principle, allows us to take into account also the influence of turbulent fluctuations on the GAM dynamics (which will be the subject of a future paper). Moreover, we note that another analogy between the Helmholtz equation and the Schrodinger equation makes it possible to adopt a quantum mechanical approach to the description of the GAM dynamics[21].

By considering an inhomogeneous index of refraction arising from the radial profile of the equilibrium temperature, we have studied the evolution of a GAM packet describing at the same time the spreading and the radial propagation of the packet. These considerations can be summarized in Fig.1 which shows the time evolution of the module of GAM radial electric field for a radially extended wavepacket, with a non-uniform radial profile of temperature. The gyrokinetic simulation has been performed by assuming inverse aspect ratio $\epsilon = 0.1$, $L_r = 320$, flat safety factor and density profiles and temperature gradient $k_T = -(1/T)(dT/dr) = 13$ with r normalized to the minor radius, which for this case is $a = 0.13m$. Hereafter, the radial coordinate is normalized to the tokamak minor radius a. Thus, the time-space (t, r) plane shows, both the bend of the signal due to the temperature gradient and the divergent character of the GAM that is similar to that of a laser beam propagating in an inhomogeneous medium.

However, in the figure we distinguish further characteristics of the GAM evolution. The region between $0.5 < r < 0.6$ shows a rapid damping of the signal, whereas in the range $0.4 < r < 0.5$ the mode propagates maintaining a coherent structure like a soliton. Moreover, the bottom panel of Fig.1 shows that the amplitude of the electric field in the (t, r) plane exhibits a modulation in the coherent part of GAM that propagates. We will now apply optical theory to demonstrate that these behaviours are due to the second radial derivative of n_G directly related to the equilibrium temperature profile via ω_G and ρ_i, and will then discuss the implications of these effects on GAMs in real tokamaks.

A. Eikonal theory

In order to isolate effects related to the radial temperature profile, we consider the eikonal equation $(\nabla s)^2 = n^2$, where s is the wave phase associated to the curvature of the wave front $R = 1/s$ which makes it possible to describe the behavior of a light beam traveling in a medium with a refraction index varying "slowly" with position. In order to give a intuitive picture of the problem, we initially neglect diffraction effects[18,19] and observing that light rays are defined as lines perpendicular to the wave front $s(x, y) = constant$, we write the eikonal equation

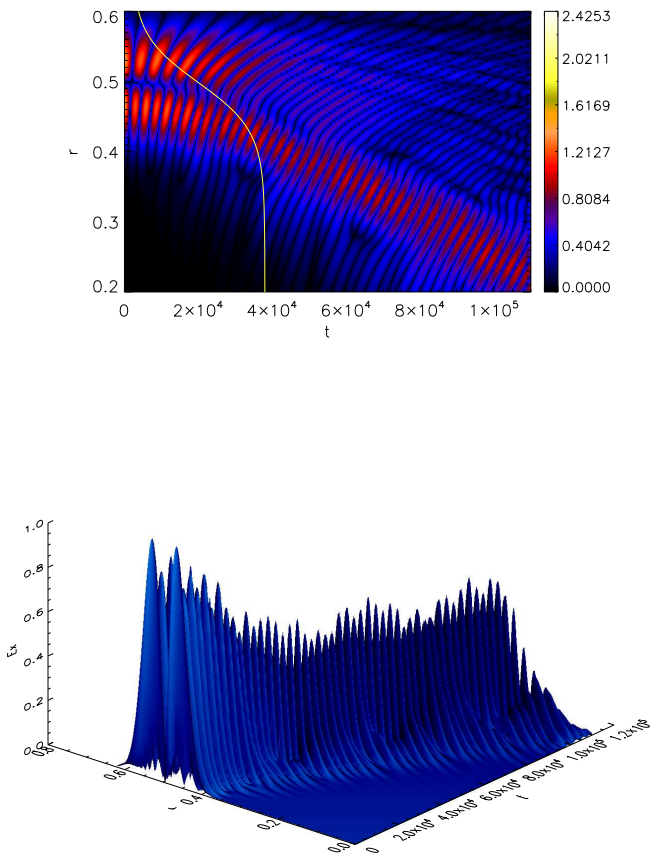

FIG. 1. *Time evolution of GAMs with an inhomogeneous profile of temperature. The top panel shows the spreading of the signal and the bend of the GAM node starting at* $r_0 = 0.5$ *due to the temperature profile. The latter is overplotted in yellow. The bottom panel shows the amplitude modulation of the GAM.*

in the vector form[20]:

$$\frac{d}{d\tau}(n\frac{d\mathbf{r}}{d\tau}) = \nabla n \tag{6}$$

where $d\tau$ is the curvilinear element along the ray and where $\mathbf{r}$ is the position vector of a generic point on the ray. By adopting the configuration indicated in Fig. 1 in Ref. 18, we use the optical approximation $d\tau = dx$ (temporal direction of GAM) based on the fact that we assume our beam remains near some axis in space. We decompose the vector $\mathbf{r} = x\hat{\mathbf{e}}_x + y\hat{\mathbf{e}}_y$ into the two components on the fixed axis and write:

$$\frac{d}{dx}\Big[n\Big(\frac{dx}{dx}\Big)\hat{\mathbf{e}}_x + n\Big(\frac{dy}{dx}\Big)\hat{\mathbf{e}}_y\Big)\Big] = \frac{\partial n}{\partial x}\hat{\mathbf{e}}_x + \frac{\partial n}{\partial y}\hat{\mathbf{e}}_y \tag{7}$$

In the framework of the optical approximation, and for the goal of this paper, we consider that the refraction index n is constant along the x direction. By assuming a Gaussian packet with centre y_0 we obtain:

$$n\frac{d^2}{dx^2}y_0(x) = \frac{\partial n}{\partial y}\Big|_{y_0} \tag{8}$$

By neglecting diffraction effects we can assume that a generic radial point of the gaussian packet moves with the same law:

$$n\frac{d^2}{dx^2}y_1(x) = \frac{\partial n}{\partial y}\Big|_{y_0} + (y_1 - y_0)\frac{\partial^2 n}{\partial y^2}\Big|_{y_0} \tag{9}$$

where we have used a Taylor expansion to connect $\partial n/\partial y$ calculated in y_0 and y_1 respectively. In this way it is possible to model the evolution of the width W of a narrow wavepacket, using $y_0(x)$ and $y_1(x)$ to represent the trajectories of the centre and edge of the wavepacket with $W(x) = y_1(x) - y_0(x)$. By subtracting Eq. 9 from Eq. 8 we obtain:

$$n\frac{d^2}{dx^2}W(x) = +W\frac{\partial^2 n}{\partial y^2}\Big|_{y_0} \tag{10}$$

This equation can be completed by adding the diffraction term in order to obtain an equation of motion for the beam radius:

$$n\frac{d^2}{dx^2}W(x) = +W(x)\frac{\partial^2 n}{\partial y^2}\Big|_{y_0} + \frac{1}{nc^2W(x)^3} \tag{11}$$

where c^2 is a constant related to the properties of the medium[35,36]. Thus, we have obtained equations of motion for the time evolution of the central beam radial position (see Eq. 8) and for the time evolution of the beam width (see Eq. 11). We note that the diffraction term in Eq. 11 can be justified rigorously using the complex eikonal approach[18,19,38]. Here, we also note that Eq. 11 is an Ermavok equation[34] which represents the real part of the complex Riccati equation used in different domains of physics such as cosmology, quantum mechanics, optics and so on:

$$\frac{d}{dx}S(x) + S(x)^2 + \Omega^2 = 0 \tag{12}$$

where S is the complex quantity $S = s + i\phi$. From complex eikonal theory we recall that s is related to the radius of curvature of the wavefront, whereas the imaginary part is related to the width $\phi = 2/W^2$ of the wave packet. By substituting the S relation in Eq. 12 it is possible to see that the imaginary part of the obtained expression leads to $s = d/dx[\ln W(x)]$. When this latter expression is substituted in the real part of the Riccati equation, we obtain Eq. 11. Further details can be found in the appendix in which it is shown how the same results of this section can be obtained in the framework of the paraxial WKB method. We observe that the two equations Eq. 8 and Eq. 11 are independent, which implies that the centre trajectory and the width W quantity are uncorrelated.

We recall that we have already studied for GAMs the competition between the first derivative k_T of temperature and diffraction effects[18]. We have quantified the effects related to k_T that produce an increase of the radial

group velocity and a bend in the wave front in the space time plane that corresponds to the phase mixing[22,33,42]. At the same time we have estimated the diffraction effects that generate a spreading of the energy GAM packet.

B. Eikonal equation applied to GAMs

In this section we apply the eikonal theory to the GAM behaviour. By recalling the coordinate relations $x = \omega_G t$ and $y = r/(\sqrt{\alpha_1}\rho_i)$ and that the GAM refractive index is related to the temperature profile we can rewrite Eq. 10 as follows:

$$\frac{1}{\omega_G^2}\frac{d^2}{dt^2}w_G(t) = +w_G(t)\alpha_1\rho_i^2 \left[\ a_2\Big(\frac{1}{T}\frac{dT}{dr}\Big)^2\Big|_{r_0} + a_3\frac{1}{T}\frac{d^2T}{dr^2}\Big|_{r_0}\right] \tag{13}$$

where w_G represents the width of the GAM packet and where the two terms related to the temperature gradient are obtained by considering the second derivative of the refractive index with respect to r. A derivation of the coefficient, whose values are respectively $a_2 = -1/4$ and $a_3 = 1/2$ can be found in the appendix. Thus, by using the diffraction term for the GAM dynamics that we have obtained and studied in Refs. 18 and 19, we can complete the evolution equation for w_G:

$$\frac{d^2}{dt^2}w_G(t) = +w_G(t)\alpha_1\omega_G^2\rho_i^2 \Big[-\frac{1}{4}\Big(\frac{1}{T}\frac{dT}{dr}\Big)^2\Big|_{r_0} + \frac{1}{2}\frac{1}{T}\frac{d^2T}{dr^2}\Big|_{r_0}\Big] + \frac{(2\alpha_1\omega_G\rho_i^2)^2}{w_G^3} \tag{14}$$

As mentioned, in Refs. 16 and 18 it has been shown that the effect of first derivative of temperature is related to a radial acceleration of GAMs. Consequently in order to maintain the GAM in a fix radial position, and to study the effects related to the second derivative of the temperature profile and its competition with diffraction term related to the spreading of the GAM, we consider the following temperature profile for both ion and electrons:

$$T(r) = Ae^{-\frac{(r-r_0)^2}{w_T^2}} + B \tag{15}$$

In this way we have the first radial derivative of T equal to zero around the point r_0. Moreover, expression 15 will be useful in the following to compare the width of the GAM packet w_G with the parameter w_T which is directly related to the second derivative of the temperature with which we can associate a parabolic index of refraction around r_0. Taylor expanding Eq. 15 around $r = r_0$ gives:

$$T(r) \approx T(r_0) + \frac{1}{2}\frac{\partial^2 T}{\partial r^2}(r-r_0)^2 = (A+B) - \frac{A}{w_T^2}(r-r_0)^2 \tag{16}$$

and consequently we have:

$$h_T = \frac{1}{T}\frac{\partial^2 T}{\partial r^2}\Big|_{r_0} \approx -2\frac{A}{A+B}\frac{1}{w_T^2} \tag{17}$$

Eq. 14 has the following analytical solution:

$$w_G(t) = w_{G_0}\Big[\cos^2\Big(\Omega_M t\Big) + \frac{1}{(\Omega_M t_R)^2}\sin^2\Big(\Omega_M t\Big)\Big]^{1/2} \tag{18}$$

where w_{G_0} is the initial width of the GAM packet and Ω_M^2 is equal to:

$$\Omega_M^2 = \alpha_1\omega_G^2\rho_i^2\Big(-\frac{1}{4}k_T^2 + \frac{1}{2}h_T\Big)\frac{A}{A+B}\frac{1}{w_T^2} \tag{19}$$

Further, in Eq. 18, t_R is the Rayleigh range or collimation time that characterizes the divergent nature of the optical beam that we have already calculated in Ref. 18:

$$t_R = \frac{w_{G_0}^2}{2\alpha_1\omega_G\rho_i^2} \tag{20}$$

With the considered temperature profile we have $\Omega_M = \omega_G\rho_i\sqrt{-\alpha_1 A/[(A+B)w_T^2]}$. Thus, the explicit expression for Eq. 18 is:

$$w_G(t) = w_{G_0}\Big[\cos^2\Big(\frac{\omega_G\rho_i}{w_T}\sqrt{-\frac{\alpha_1 A}{A+B}}t\Big) + 4\frac{\alpha_1(A+B)}{A}\frac{w_T^2\rho_i^2}{w_{G_0}^4}\sin^2\Big(\frac{\omega_G\rho_i}{w_T}\sqrt{-\frac{\alpha_1 A}{A+B}}t\Big)\Big]^{1/2} \tag{21}$$

We have now established a parallel between the time evolution of the width of a GAM packet and the spatial profile of a laser beam that propagates in a medium with a parabolic index of refraction. Thus, Eq. 18 and Eq. 21 show a modulation behavior of the GAM packet when Ω_M is real. It is important to note that where Ω_M^2 is negative, the signal is evanescent indicating the disappearance of GAMs. This implies that there are zones related to the equilibrium profile in which the existence of GAMs could be forbidden. These considerations will be investigated in the next sections with a direct comparison between theory and simulations and afterward by analysing some experimental data in order to quantify the importance of this phenomenon in tokamak devices.

IV. SIMULATION RESULTS AND PHYSICAL INTERPRETATION

In this section, by using the gyrokinetic code ORB5, we verify analytical results obtained in the previous section. In the regime with $\tau_e \approx 1$, dispersion effects are dominated by dissipation effects due to Landau damping and by Phase-mixing Landau damping (PL) mechanism. Thus, initially we investigate the modulation of the GAM amplitude in a regime in which dissipative effects are negligible (large value of τ_e) in order to focus attention on

dispersion. After verifying the modulation behaviour of GAMs, the theory will be applied to predict modulation of the GAM in a range of parameter values of interest for tokamak devices. GAM frequency modulation is of interest in the nonlinear regime where dissipation effects may compete with drive and, in principle, linear dispersion becomes important to predict the correct GAM dynamics. We note that all the simulations discussed in this paper have been performed in the linear regime. Results in the nonlinear regime will be presented in a future paper. We begin by presenting simulations in the range between $6 \lesssim \tau_e \lesssim 40$. On the basis of Eq. 19 the possible condition for the existence of GAM is given by the dimensionless parameter:

$$C_e = \alpha_1(-\frac{1}{4}k_T^2 + \frac{1}{2}h_T) > 0 \tag{22}$$

It is important to emphasize that this constraint in our approximation has been obtained by not considering nonlinear regime and then not taking the drive into account. For our choice of profiles in Eq. 15 we can rewrite Eq. 22 as follows:

$$C_e = -\alpha_1 \frac{A}{A+B}\frac{1}{w_T^2} > 0 \tag{23}$$

We recall from Ref. 32 and Ref. 33 that α_1 is negative for $\tau_e \gtrsim 6$ and consequently we need to consider $h_T > 0$. We consider a tokamak with a major radius $R = 1.3$ and a minor radius $a = 0.13$. As we have demonstrated in Ref. 18, the applicability of optical techniques allow us to describe GAMs by using a high-order Hermite function. Thus, we can use either first order (Gaussian packets) or second order Hermite functions for the GAM electric field, depending on the emphasis that we would like to give to a particular aspect. In order to perform a systematic study of the GAM width evolution we define a Gaussian profile with a radial width w_G of the packet:

$$\phi_G = e^{-(r-r_0)^2/w_G^2} \tag{24}$$

We consider a temperature profile with $A = 0.8$ and $B = 0.2$ in Eq. 15 to have $T_0 = 1$ in the middle of the box. Setting a finite B avoids numerica problems at the boundary. In the first instant we choose $\tau_e = 40$ in order to neglect the Landau damping. We consider flat density and safety factor profiles for all the simulations. The effects of density gradients will be investigated in a future work.

We vary the GAM width in the range $0.02 < w_G < 0.08$, setting this to be smaller than the temperature width $0.1 < w_T < 0.2$ (see Eq. 15). Hereafter, we consider a GAM packet and a temperature profile centered at the same position by choosing for simplicity $r_0 = 0$. In this way, we avoid any radial motion of the peak of the GAM potential that we recall is determined by Eq. 8 related to the first derivative of the refractive index. This means that the corresponding node of the electric field will be fixed in time at $r_0 = 0$ and we focus on the shape evolution of the packet. Fig. 2 shows the time evolution of three GAM electric field signals with

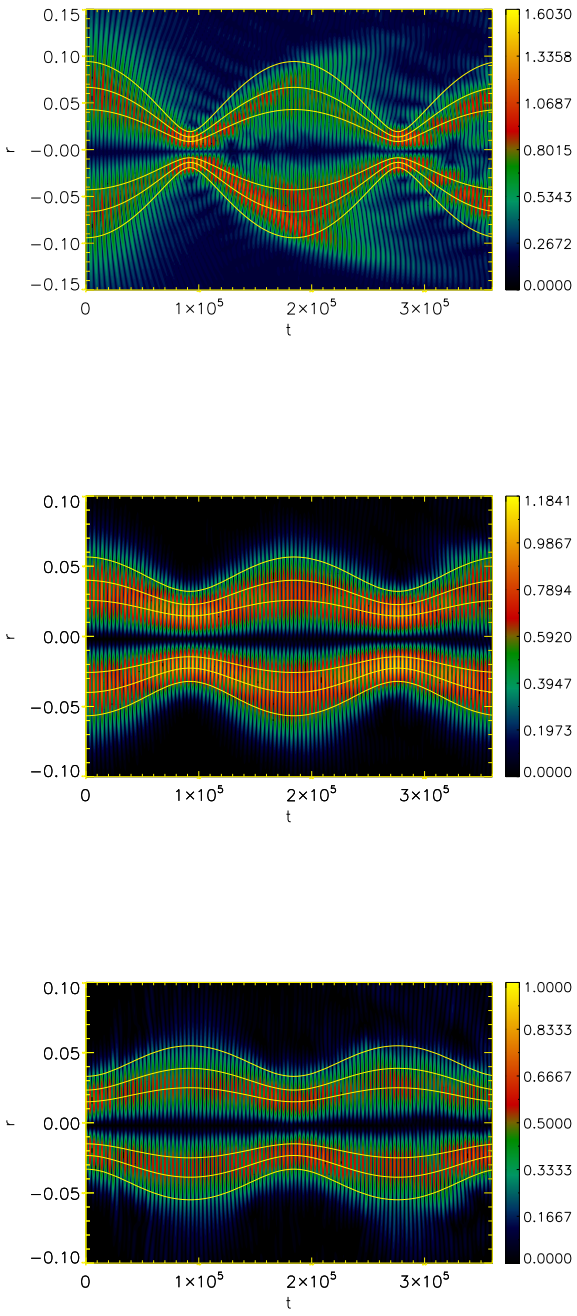

FIG. 2. *Time evolution of the module GAM electric field profile oscillating in an equilibrium with* $w_T = 0.14$. *The considered values for GAM width are* $w_G = 0.08, 0.048, 0.028$ *from top to bottom panel. Superimposed on the GAM signal, phase-path trajectories (orange lines) predicted analytically by Eq. 21 reproduce well the modulation of GAM.*

$w_G = 0.08, 0.046, 0.028$ from top to bottom panels respectively in an equilibrium temperature with $w_T = 0.14$, also overploted is the GAM width evolution predicted by Eq. 21, which shows a good agreement between simulations and analytical theory. We can give the following physical interpretation of the phenomenon. The GAM packet oscillates in an environment whose influence on the GAM structure is determined by the radial profile of the associated refractive index. During a period $t_G = 2\pi/\omega_G$ the environment acts as a lens on the GAM oscillation. If the beam size w_G is such that it compensates the focusing effects of the lens, the beam size remains constant and we can talk about a steady-state or a GAM "eigenmode" with a width $w_{G_{eig}}$. In the general case the GAM width does not match the Gaussian "eigenmode" determined by equilibrium profiles. If the input beam is initially smaller than the steady-state GAM width then the diffraction spreading for this smaller beam will then be stronger than the refocusing produced by the temperature profile. The width $w_G(t)$ will therefore begin to grow, and the Gaussian beam will begin to spread with time. As soon as its width becomes larger than the "eigenmode" extension, the opposite condition will prevail, and the beam will be refocused again. Thus, an initial beam with a width $w(t)$ larger or smaller than the steady state value $w_{G_{eig}}$ will oscillate periodically inward and outward about the steady state value in a sausage-like fashion as shown in Fig. 2.

In order to better quantify this behavior we observe that the maximum and minimum radius occur when $dw_G/dt = 0$. Some simple algebra using Eq. 18 - Eq. 20 from our theory we obtain the maximum and minimum packet widths:

$$w^2_{G_{max}} w^2_{G_{min}} = \frac{4\alpha_1 \rho_i^2}{-1/4k_T^2 + 1/2h_T} \tag{25}$$

that for the case considered in our simulation corresponds to haveing $w^2_{G_{max}} w^2_{G_{min}} = -4\alpha_1 \rho_i^2 w_T^2 (A+B)/A$. We conclude from this that the product of the maximum and minimum radii is a constant, independent of the entrance conditions of the beam. The condition to obtain a GAM eigenmode oscillation can be found directly from Eq. 25.

$$w_{G_{eig}} = \Big[\frac{4\alpha_1}{-1/4k_T^2 + 1/2h_T}\Big]^{1/4} \sqrt{\rho_i} \tag{26}$$

By considering $k_T = 0$, $\alpha_1 = -8.9$, $A = 0.8$, $B = 0.2$, $\rho_i = 1.9 \cdot 10^{-3}$ and $w_T = 0.14$ we obtain for this case that the width for an eigenmode GAM packet is $w_{G_{eig}} = 0.04$. Thus, in the case with $w_G < w_{G_{eig}}$ (bottom panel of Fig. 2) the packet first expands and then contracts in a repeating cycle. For the cases $w_G > w_{G_{eig}}$ the GAM is initially focused (top and central panel of Fig. 2). The expression 25 shows also that the product of the maximum and minimum of the GAM width depends on the characteristics of the local environment. This implies that a larger minimum width GAM should be associated with a smaller maximum radial spread, as it is evident in comparing the top and middle panels of Fig.2. It is important to note that energy during the oscillation behavior is conserved and consequently the amplitude of the GAM strongly increases when it reaches $w_{G_{min}}$ producing strong variations in the GAM signature that we can associate with bursts. The amplitude of the GAM is shown using the color bar in the figures and is maximum when w_G is minimum. The color bar is normalized to 1 by considering the maximum value of the initial signal at $t = 0$. Fig. 3 shows Ω_M^{-1} of the modulation as a function of $w_T L_r^2$ and demonstrates that the simulation results show a direct proportionality between these two quantities. This result can be interpreted by observing that $L_r^2 \propto T_i$ via the ρ_i^2 dependence and $\Omega_M^{-1} \propto T_i$ via the dependence on $\omega_G \rho_i$. These considerations are confirmed in Fig. 4 in which show the module of the electric field evolution of a packet as a result of the competition between the second derivative of the temperature and the gaussian beam of the GAM for three case $L_r = 320$ (top), $L_r = 640$ (centre) and $L_r = 960$ (bottom). The ORB5 simulation results are compared with the theory predictions of the GAM width (yellow lines superimposed on the simulation signal in Fig. 2 and Fig. 4). All cases in Fig 4 demonstrate that the maximum amplitude is achieved at the minimum width, with $L_r = 2/\rho^* = 960$ being particularly striking. Moreover, we can distinctly observe a curvature of the wave front of the GAM in time. We emphasize that this curvature is produced in a time-space plane and, as discussed in previous the section, is equal to $1/R(t) = d \ln W(t)/dt$ whose explicit expression is:

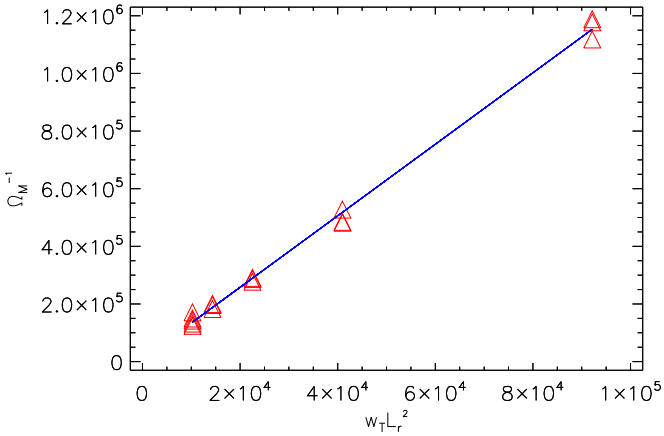

FIG. 3. *Plot of Ω_M^{-1} (proportional to the period of the GAM modulation) as a function of $w_T L_r^2$. The direct proportionality between these quantities is in agreement with the prediction of Eq. 21.*

$$R(t) = \frac{t_R^2 \Omega_M^2 \cot(\Omega_M t) + \tan(\Omega_M t)}{\Omega_M (1 - \Omega_M^2 t_R^2)} \tag{27}$$

This curvature, that changes concavity periodically in time, corresponds to a periodically modulation of GAM

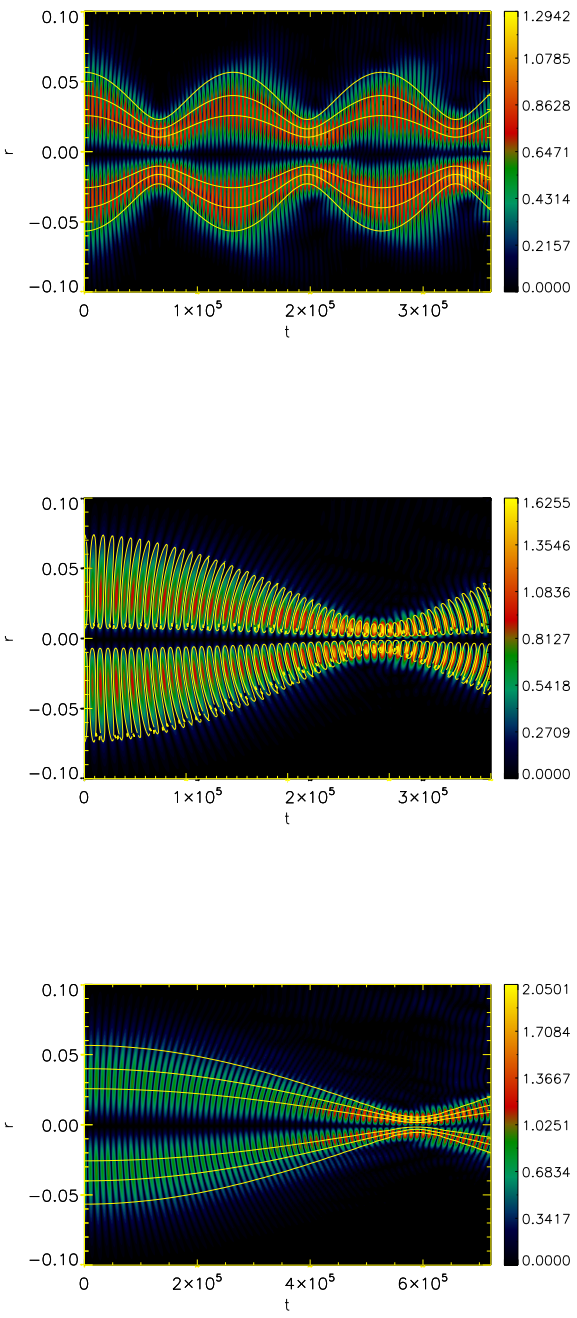

FIG. 4. *Time evolution of the module of GAM electric field profile with* $w_G = 0.048$ *oscillating in an equilibrium with* $w_T = 0.14$. *From top to bottom panel* $L_r = 320, 640, 960$. *For* $L_r = 320$ *and* $L_r = 960$, *superimposed on the electric field module, phase-path trajectories (orange lines) predicted analytically by Eq. 21 well reproduce the modulation of the GAM. For* $L_r = 640$, *superimposed on the GAM signal, there are isocontours of the packet obtained by considering the wave front described in Eq. 27.*

frequency that has been observed in different experiment (in the absence of bursts)[15]. Comparison between simulations and prediction from Eq. 27 is shown in Fig. 4 for the case $L_r = 640$. If we consider a cut of electric field signal along the time direction and we perform the Fourier transform we observe a splitting of the frequency starting from the principal frequency ω_G. We recall that splitting of frequency is not a fully understood characteristic of GAMs observed in experiments. Moreover, we note that recently in Ref. 8 a GAM has been observed to split into two parts moving in opposite directions. This behavior can be explained in geometrical optics as a diffraction effect of the GAM due to equilibrium profiles. We observe that the temperature gradient investigated in Ref. 16 and Ref. 18 bends the wave front of the GAM in the time-space plane (t, r) via a Phase-mixing effect[22,42], while the second derivative of temperature profile and the dispersive effect curves the wave front. For completeness, we also perform simulations in which the C_e condition is negative. As explained, for a negative value of C_e, the initial GAM packet should disappear. The simulation (not shown) demonstrates that in this case the initial signal spreads very rapidly and the packet disappears in a time shorter than the Raylegh time t_R. Thus, we have demonstrated the validity of our approach to the GAM description in a range in which dissipative effects are negligible. If we perform a generic simulation in a regime of interest for tokamaks and consequently with $\tau_e \approx 1$, the effect of dissipation linked to Landau damping is so strong that we observe the classical signal decaying monotonically in time. However, by using Eq. 19 we can perform a simulation with specific parameter values that make it possible to demonstrate the modulation effects also in the presence of the Landau damping. By considering that α_1 is positive for $\tau_e < 6$ we choose $A = -0.4$ and $B = 1.4$ in order to have a positive $h_T(0)$ with $T(0) = 1$. We recall the condition to obtain a GAM oscillation expressed in Eq. 23. By considering a value $\tau_e = 1$ we obtain a positive $\alpha_1 = 1.9$ We consider $L_r = 1441$, $a = 0.5m$, $R = 1.65m$ that corresponds to the AUG value with an $\epsilon = 0.3$. By choosing an ad-hoc value $w_T = 0.075$ and $w_G = 0.06$, in Fig. 5 we are able to show the time evolution of the GAM signal in which Landau damping and the modulation frequency are observed at the same time. The importance of the mechanism that we describe becomes apparent when we consider realistic nonlinear simulations. In these cases, the GAM is driven by turbulence, compensating the effects of the Landau damping. Consequently the mechanism of focusing/spreading previously discussed can play a very important role in the modulation of GAMs. However, we note that a similar nonlinear competition between drive and dissipation could in principle generate a GAM intermittent oscillation. In this case, our work may helps to distinguish the two effects, isolating the action of drive sources.

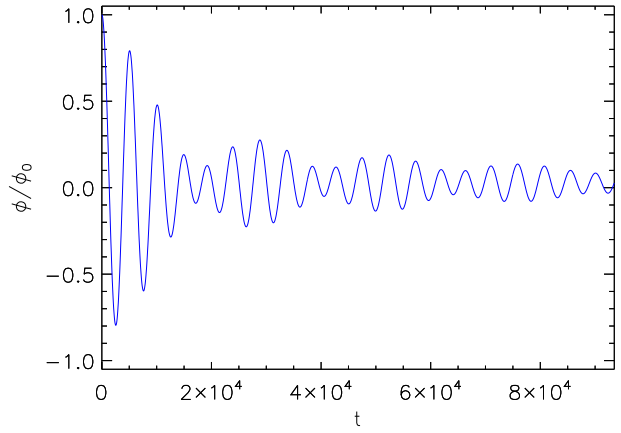

FIG. 5. *Time evolution of peak of the GAM electrostatic potential at r_0 showing how the Landau damped signal is modulated in amplitude due to the curvature of the temperature profile. For this case $w_T = 0.075$ and $w_G = 0.1$ have been used in order to illustrate the effect, which would otherwise have been masked by Landau damping.*

V. MODULATION IN REALISTIC PARAMETER VALUES

In this section we apply the modulation theory to the behaviour of GAMs observed in experiments. The principal goal is to provide rough estimates from our theoretical model of the GAM amplitude and frequency modulation that might be expected from the parameters in the experiment. The experimental comparison is taken from AUG discharge #29722, a circular ($\kappa \sim 1.1$), limiter L-mode with 400 kW of central ECRH heating, $B_0 = -2.4$ T, $I_p = 0.6$ MA, $q_{95} \sim 4$, core density $n_{e0} \sim 2 \times 10^{19}$ m^{-3} and $T_{e0} \sim 3$ keV[43]. GAMs and plasma flow oscillations have been studied extensively on AUG using microwave Doppler reflectometry (DR)[25]. From the Doppler shifted peak frequency in the backscattered signal $f_D = u_\perp k_\perp/2\pi$ and the Doppler peak amplitude $A_D \propto \delta n_e$ one obtains radially localized measurements of the perpendicular flow (dominated by the $E_r \times B$ velocity) and density turbulence[15,44]. Fig. 6(a) shows flow velocity (green) and density fluctuation (red) spectra from the edge region $\rho_{pol} \sim 0.962$ of AUG shot #29722. The GAM $m = 0$ flow oscillation appears as the coherent peak around 15.8 kHz in the f_D spectra. The weaker peak in the A_D spectra arises in these circular plasma shapes due to the DR probing line of sight being well below the flux surface magnetic axis, making the DR peak amplitude sensitive to the GAM $m = \pm 1$ pressure sideband. Note the absence of any low-frequency ZF feature in this discharge. Radially the GAM is most strongly localized to the edge, as shown in Fig. 6(b) by the P_{GAM} (purple) points, across the negative E_r shear region, as illustrated in Fig. 6(c). In this circular, limiter configured shot #29722, the GAM is observed over a fairly wide radial region of $\rho_{pol} \sim r/a$ between $r_1 \approx 0.92a$ and $r_2 \approx 0.98a$ (see Ref. 43). For divertor configurations the GAM is much more constrained to a narrow E_r shear region.

Across the GAM spatial peak region the GAM frequency f_{GAM} (green points) is constant, forming an eigenmode structure. Further inside, the GAM is weaker and its frequency follows the local sound speed, taking a on continuum-mode structure. Fig. 6(d) shows the time resolved flow spectrogram $S(f_D, t)$ as a contour plot. Here, the intermittent nature of the GAM can be observed. Both the GAM amplitude and frequency are modulated[15]. The dominant components of

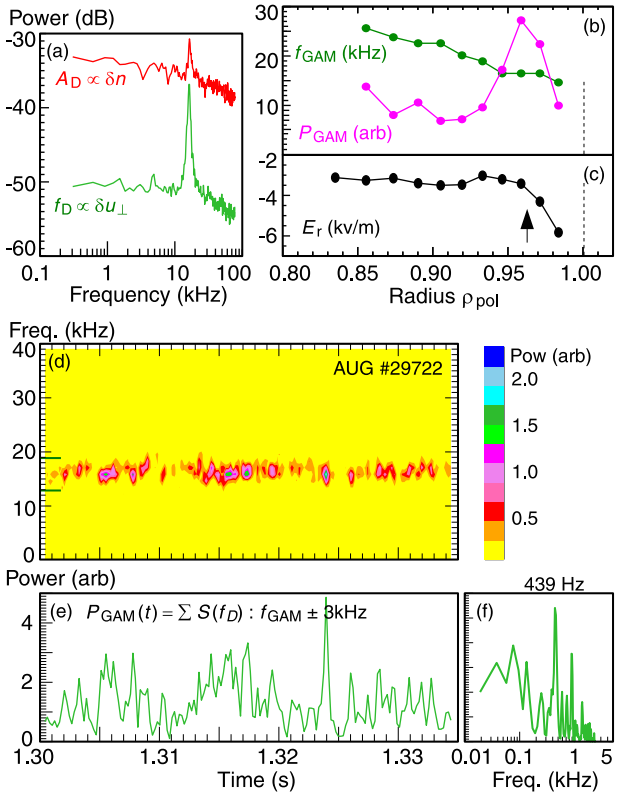

FIG. 6. *GAM evolution in L-mode, cicular limiter AUG shot #29722 revealed by Doppler reflectometry: (a) Spectra of fluctuations in Doppler peak frequency $f_D \propto u_\perp$ proportional to the perpendicular flow, and Doppler peak amplitude $A_D \propto \delta n$ at radius $\rho_{pol} = 0.965$, (b) radial profiles of GAM frequency f_{GAM} and magnitude P_{GAM} plus (c) radial electric field E_r, (d) time resolved spectrogram $S(f_D, t)$ of plasma flow f_D, (e) time trace of integrated GAM frequency peak $P_{GAM}(t)$, and (f) spectrum of $P_{GAM}(t)$.*

the GAM flow modulation are obtained by integrating the $S(f_D, t)$ spectrum over the GAM peak frequency range $f_{GAM} \pm 3$ kHz, as shown in $P_{GAM}(t)$ trace in plot Fig. 6(e), and then taking its spectrum as shown in Fig. 6(f). The GAM flow amplitude modulation has a dominant peak around 440 Hz, with a slower deeper modulation around a few tens of Hz. It should be noted that the GAM modulation spectrum changes moderately over

a period of tens of milliseconds as the discharge conditions drift. Nevertheless, a dominant modulation of a few hundred Hz is most common in AUG discharges cf. 15. Generally, it has been found over a range of discharges that the GAM modulation can be either rather coherent with a sinusoidal-like amplitude variation (up to 50 % p.t.p. modulation), or more abrupt with an intermittent nature (100 % modulation), as well as exhibiting a strong frequency chirping[2]. The latter feature is more suggestive of an intermittency in the GAM drive.

As in the experiment, the same temperature profile for electrons and ions is assumed, ie. $\tau_e = 1$. This means that the α_1 term (see Eq. 3) linked to the second order effects is positive and equal to $\alpha_1 = 1.9$. In this deuterium plasma $\Omega_i = 1.15 \times 10^8 rad/s$ and by assuming as a reference an intermediate temperature $T = 150eV$ for the region of interest one obtains $v_{th} = 1.2 \times 10^5 m/s$ and $\rho_i = 1.05 \times 10^{-3} m$ and a GAM frequency $\omega_G/\Omega_i = 1.05 \times 10^{-3}$ which corresponds to $f_G = \omega_G/(2\pi) = 19.2kHz$. Fig. 7 shows profiles of h_T and k_T for the shot #29722 with peak values $h_{T_p} \approx 190$ and $k_{T_p} \approx 13$ respectively.

As we can see, the condition $C_e > 0$ (Eq. 22) is satisfied in the region in which the GAM was observed. The values of the prinicple plasma parameters for this shot are listed in the top line of Table I. For these parameter values, using Eq. 26, we expect a GAM eigenmode with a size $w_{G_{eig}} = 1.4cm$. The maximum extension of the GAM observed in the experiment is around $w_{G_{max}} = 2.5cm$ and on the basis of our model a variation in the amplitude should be expected as a consequence of the fact that $w_{G_{min}} = w^2_{G_{eig}}/w_{G_{max}} = 0.78cm$. This variation is indeed observed in the GAM signal as shown in Fig. 6(d). Using the values of Table I in Eq. 19 we can estimate an $\Omega_M \approx 5.26 \times 10^3 rad/s$, which corresponds to a $f_M = \Omega_M/(2\pi) \approx 400Hz$. By considering only the h_T term in Eq. 19 we have $f_M = \Omega_M/(2\pi) \approx 540Hz$. These values are of the same order of magnitude as generally observed in the experiments.

In order to better understand the results of the experiment, we recall that in the literature we distinguish between an eigenmode GAM and a continuum GAM. In Ref. 21 the generation of an eigenmode GAM has been demonstrated as a competition between nonlinear effects and spreading of GAM in flat equilibrium profile conditions. In the present work we have shown the linear existence of a GAM eigenmode as a function of a nonuniform temperature equilibrium profile. Although these works help to better understand the characteristics of GAMs, further effort is required to achive a complete understanding of the eigenmode description of GAMs in general realistic situations. When GAMs "see" the continuum, they exhibit a radial oscillation frequency that depends on the temperature profile. This leads to the generation of the well understood phase-mixing effect[22,33,42]. One of the consequences related to phase-mixing is a radial drift movement of the GAM with an acceleration equal to $a_c \approx 0.5\alpha_1\omega_G^2\rho_i^2 k_T/a$ as a direct

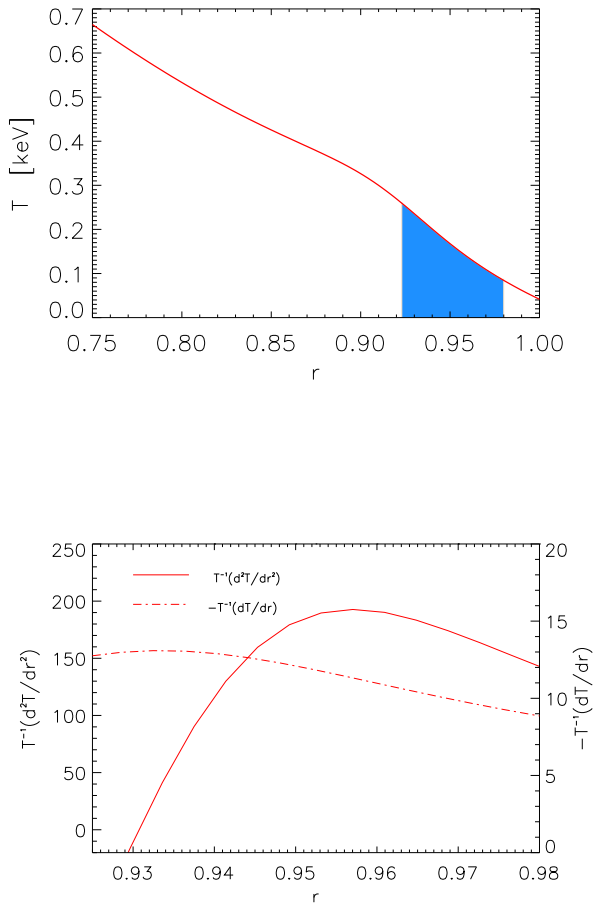

FIG. 7. *Top: temperaure profile with blue region indicating where a GAM was observed in AUG shot #29722. Bottom: corresponding first and second derivatives of the temperature profile in the region in which GAM is developed.*

consequence of the temperature gradient[16]. Using the parameter values for the specific analysed shot we obtain $a_c = 3.9 \times 10^5 m/s^2$. This means that the GAM packet would leave the region of interest $0.92 < r < 0.98$ in a time $\delta t = \sqrt{2S/a_c} = 3.8 \times 10^{-4}$s. This suggests that the GAM wavepacket should leave the region before any modulation due to the temperature equilibrium profile could be observed. However, we note that in the considered shot we are in the presence of an eigenmode structure with a modulation spectrum that changes moderately over a period of tens of milliseconds during the which the GAM can be modulated at different rates on the basis of the calculated frequency f_M. In any case, we use profiles of the shot principally to provide an order of magnitude estimate of the modulation frequency. We have shown that this value is compatible with observed

TABLE I. Values of parameters for the AUG shot #29722 (L-mode) and #34954 (H-mode): The electron T_e is assumed equal to T_i temperature, α_1 for $\tau_e = 1$, axial magnetic field B_0, Larmor radius ρ_i, ω_G, normalized temperature gradients h_T and k_T and C_e coefficient

Regime	$T_i(eV)$	τ_e	α_1	$B_0(T)$	$\rho_i(m)$	ω_G/Ω_c	h_T	k_T	C_e
L-mode	150	1.0	1.9	2.4	$1.0 \cdot 10^{-3}$	0.001	190.0	13	> 0 (GAM osc.)
H-mode	358	1.0	1.9	2	$1.3 \cdot 10^{-3}$	$1.3 \cdot 10^{-3}$	-420	15	< 0 (no GAMs)

values in the experiment, and we postpone a deeper analysis of the experiments in the framework of the present theory to a future article.

Before discussing the H-mode regime, we recall the principal GAM characteristics observed during the L-H transition. As the transition is approached it is possible to observe the following events[45]:

- The radial extent over which the GAM exists narrows with the increasing radial electric field E_r.
- The GAM generated zonal shearing interact with the broadband background fluctuations.
- The GAM spectral peak generally appears continuous in time, although its amplitude tends to be modulated by up to 50% or more, giving the appearance of a stream of bursts.
- Both the GAM frequency and its amplitude, tend to rise as the H-mode transition is approached.
- The GAM signal disappears when the plasma enters H-mode.

This description is qualitatively consistent with what is predicted by the model presented in the previous sections. In fact, during the L-H transition the temperature at the edge increases, and truss correspondingly to an increase of the modulation frequency (see Eq. 19). The change of the modulation frequency is also determined by the changes in k_T and h_T. Moreover, there is a change of concavity of the temperature profile moving towards the H-mode, for which the condition $C_e > 0$ becomes satisfied more and more in a narrower region. Thus, also the GAM width should decrease. These changes are further reflected in the amplitude oscillations related to the width condition (see Eq. 25). Finally, if the constraint C_e becomes negative in the entire pedestal region then the GAM structure should completely disappear. Thus, the model presented in this paper could help to understand the different aspects observed in the GAMs dynamics.

The top panel of Fig. 8 shows the edge temperature profile for the AUG shot #34954 in which an H-mode has been established. For this H-mode case we consider an indicative temperature value of the edge region around $T = 358$ eV and, by assuming $\tau_e = 1$, with a $B_0 = 2T$ we obtain an $\Omega_i = 9.6 \times 10^7 rad/s$, $\omega_G/\Omega_i = 1.3 \times 10^{-3}$ and

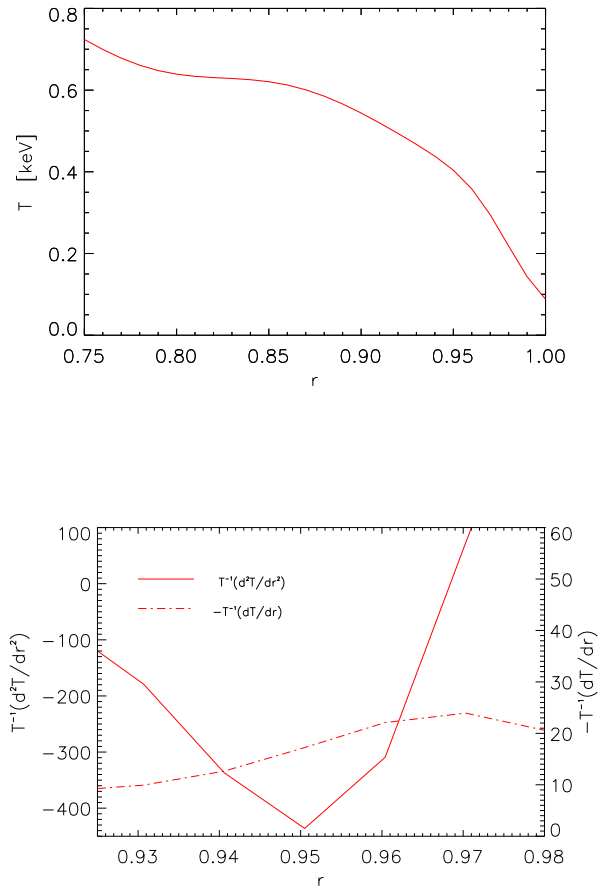

FIG. 8. *Top: Edge temperature profile for AUG shot #34954 in which an H-mode is observed. Bottom: corresponding first and second radial derivatives of the temperature profile.*

a $\rho_i = 1.3 \times 10^{-3}$ m. The bottom panel of Fig. 8 shows k_T and h_T quantities for the same shot. We can observe the change of concavity for the temperature profiles with respect to that of the previos L-mode shot. Using the profiles of k_T and h_T in Eq. 19 we deduce that the existence of a GAM for which $C_e > 0$ is limited to $r > 0.98$, then in a very narrow region close to the limits of the tokamaks. The principal values for this H-mode case are summarised in Table I. It is important to note that GAMs are ob-

served in the I-mode. In this regime GAMs exhibit a strongly intermittent behaviour with strong fluctuations. This regime is characterized by a temperature gradient similar to that of the H-mode but with a density gradient similar to that of L-mode. The difference between H-modes and I-modes needs to be further explored. It is possible that a different combination of k_T and h_T could be involved in determining the GAM dynamics in these regimes. However, having clear approximations in which Eq. 22 have been derived, the differences between these regimes suggest that further studies (similar to those on the current sample of experimental shots) should be made to understand, or to improve the validity of the criterion on the GAM existance proposed here. We recall that in Ref. 22 a model based on the competition between drive and Phase mixing-Landau damping mechanism has been proposed to explain the difference in the GAM behaviour in I- and H-modes. Analysis of how the edge profiles impact on GAMs, following the ideas outlined in this paper, could help improve our understand the challenging environment of the edge plasma. We emphasize that in the experiments the physics of the nonlinear processes of GAMs exhibit complex aspects in which several factors determine the GAM behavior. In particular the drive can compensate the damping and can interact with the dispersive effects, probably contributing to generate intermittent behaviour of GAM. However, effects described in this paper are involved in the dynamics and their investigation may help to isolate other phenomena such as the interaction between turbulence and GAMs.

VI. CONCLUSION

In this work we have studied the intermittency of GAMs. This appears as a low frequency modulation commonly observed in experiments, that can appear as a burst or as a simple sinusoidal oscillation in the intensity of the GAM. In the steady state case a modulation of the principal GAM frequency $f_G = \omega_G/2\pi$ has also been observed. In order to investigate this phenomenon we used an interesting approach already successfully applied to describe the dispersion characteristics of GAMs[18,19,21], and here we extend the capability of previous works[16,22] to describe a fuller range of GAM characteristics. In particular, the eikonal theory and laser opto-electronics methods have been successfully applied to describe the modulation behavior of GAMs.

In this work, we have demonstrated that, as well as being generated through nonlinear interactions between turbulence and GAMs, GAM modulations can also be generated by the properties of the equilibrium temperature profile. Both of these effects should be taken into account in a complete description of the GAM dynamics. In particular, we have shown that the temperature profile could play a fundamental role in defining the characteristics of the modulation amplitude and frequency of GAM. In our modelling, the modulation frequency appears as a periodic change of the phase-front of the GAM in the space-time plane, and the intermittent behavior of GAMs is determined by competition between the curvature of the temperature profile and the GAM radial extension. The competition between these two quantities could be responsible for the generation of burst-like GAM amplitudes and could also be involved in the generation of GAM eigenmode structures. Finally, we emphasize that the link established here between GAM dynamics and equilibrium profiles, maybe key to explaining how GAM dynamics varies in different plasma regimes. We have also derived a possible criterion for the existence of GAMs from the optical theory, based on the shape of the temperature profile in the region in which GAM is located. We note that this criterion has been obtained in optical approximation and we have verified it in linear global simulations. Further investigations are needed in order to verify its validity in more general experimental conditions in which nonlinear effects related, in particular to the drive, are also taken into account. However, this criterion could help to elucidate, together with the Phase mixing-Landau damping mechanism, the reason for which GAMs are not observed in H-modes. In conclusion, the description of modulations presented here is compatible with the different characteristics of GAMs observed in plasma discharges in the AUG device. We even propose that the observed GAM dynamics may prove a useful constraint in diagnosing the local equilibrium profiles.

APPENDIX: PARAXIAL WKB METHOD

In this appendix, we discuss the parallel between the eikonal theory and the paraxial WKB (pWKB) method in the framework of GAMs. We recall that equivalence between geometrical optical methods and pWKB has been established in Ref.s 39–41 and further detail for the specific GAM case can be found in Ref.s 18 and 19. In the notation of Refs. 18 and 19, the equations for the evolution of the GAM packet follow from the Hamiltonian:

$$H = F(r) + \frac{1}{2}G(r)k_r^2 = \omega_G\Big(1 + \frac{1}{2}\alpha_1 k_r^2\rho_i^2\Big) = \omega \quad \text{(A28)}$$

where $F = \omega_G$ and $G = \alpha_1\omega_G\rho_i^2$. In local equilibria where the first radial derivative of ω_G and ρ_i^2 can be neglected, we obtain the following equations of motion for the center (k_0, r_0) of the packet

$$\frac{dr_0}{dt} = H_{k_r} \to r = r_0 \qquad \frac{dk_0}{dt} = -H_r \to k_r = k_0 = 0 \quad \text{(A29)}$$

The beam envelop evolution in time is calculated by means of:

$$\frac{dS}{dt} = -H_{rr} - H_{k_r k_r}S^2 \quad \text{(A30)}$$

which is a complex Riccati equation for the beam envelope $S = s + i\phi$ with $\phi = 2/W^2(t)$ related to the width W of the packet while s is connected to the curvature of the wave front in the (t, r) space. The Riccati equation can be solved by adopting the following substitution $S = (H_{k_r k_r} p)^{-1} dp/dt$. Thus, we rewrite Eq. A30:

$$\frac{1}{H_{k_r k_r}}\Big[\frac{1}{p}\frac{d^2p}{dt^2} - \Big(\frac{1}{p}\frac{dp}{dt}\Big)^2\Big] = -H_{rr} - H_{k_r k_r}\Big(\frac{1}{H_{k_r k_r} p}\frac{dp}{dt}\Big)^2 \tag{A31}$$

Consequently we have:

$$\frac{d^2p}{dt^2} = -H_{k_r k_r} H_{rr} p \tag{A32}$$

which gives the following solution:

$$p = A\cos(\Omega_M t) + B\sin(\Omega_M t) \qquad \Omega_M = \sqrt{H_{k_r k_r} H_{rr}} \tag{A33}$$

By explicitly using expressions for $H_{k_r k_r}$ and H_{rr}:

$$H_{k_r k_r} = \alpha_1 \omega_G \rho_i^2 \tag{A34}$$

$$\begin{aligned} H_{rr} &= \frac{\partial^2}{\partial r^2}\omega_G + \frac{\alpha_1 k_r}{2}\frac{\partial}{\partial r^2}\omega_G \rho_i^2 \\ &\approx \omega_G\Big[-\frac{1}{4}\Big(\frac{1}{T}\frac{dT}{dr}\Big)^2 + \frac{1}{2}\frac{1}{T}\frac{d^2T}{dr^2}\Big] \end{aligned} \tag{A35}$$

we obtain:

$$\Omega_M^2 = \alpha_1 \omega_G^2 \rho_i^2\Big[-\frac{1}{4}\Big(\frac{1}{T}\frac{dT}{dr}\Big)^2 + \frac{1}{2}\frac{1}{T}\frac{d^2T}{dr^2}\Big] \tag{A36}$$

Then:

$$S = \frac{\Omega_M}{H_{k_r k_r}}\Big[\frac{-\sin\Omega_M t + B/A\cos\Omega_M t}{\cos(\Omega_M t) + B/A\sin\Omega_M t}\Big] \tag{A37}$$

Using an initial condition $\phi_0 = 2i/W_0^2$ we obtain

$$\frac{2i}{W_0^2} = \frac{\Omega_M}{H_{k_r k_r}}\frac{B}{A} \rightarrow \frac{B}{A} = \sqrt{\frac{H_{k_r k_r}}{H_{rr}}}\frac{2i}{W_0^2} = ib \tag{A38}$$

Thus $Im[S] = 2/W^2$ will be:

$$\begin{aligned} \frac{2}{W^2} &= \sqrt{\frac{H_{rr}}{H_{k_r k_r}}}\frac{b\sin^2(\Omega_M t) + b\cos^2(\Omega_M t)}{\cos^2(\Omega_M t) + b^2\sin^2(\Omega_M t)} = \\ &= \frac{2}{W_0^2}\frac{1}{1 + (b^2-1)\sin^2(\Omega_M t)} \end{aligned} \tag{A39}$$

that corresponds to have:

$$W^2 = W_0^2\Big[\cos^2(\Omega_M t) + \frac{4H_{k_r k_r}}{H_{rr} W_0^4}\sin^2(\Omega_M t)\Big] \tag{A40}$$

It is immediate to show that:

$$\begin{aligned} Re[S] &= \sqrt{\frac{H_{rr}}{H_{k_r k_r}}}\frac{(b^2-1)\cos(\Omega_M t)\sin(\Omega_M)t}{\cos^2(\Omega_M t) + b^2\sin^2(\Omega_M t)} \\ &= \sqrt{\frac{H_{rr}}{H_{k_r k_r}}}\frac{[4H_{k_r k_r}/(H_{rr}W_0^4) - 1]\tan(\Omega_M t)}{1 + 4H_{k_r k_r}/(H_{rr}W_0^4)\tan^2(\Omega_M t)} \end{aligned} \tag{A41}$$

In this way it is possible to establish a parallel between Eq. 18, Eq. 27 and Eq. A40, Eq. A41 respectively.

ACKNOWLEDGMENTS

Interesting and useful suggestions by K.McClements are kindly acknowledged. The authors are indebted to P.Simon and C.Angioni for data and useful discussions. Simulations were performed on the DIRAC and DRACO supercomputer. This work has been (part-) funded by the EPSRC Energy Programme [grant number $EP/W006839/1$]. To obtain further information on the data and models underlying this paper please contact PublicationsManager@ukaea.uk.

[1] N. Winsor, J. L. Johnson, and J. M. Dawson, *Phys. Fluids* **11**, 2448 (1968).
[2] G.D. Conway, A.I. Smolyakov and T. Ido, *Nucl. Fusion* **62**, 013001 (2022).
[3] K. Itoh, S-I. Itoh, P. H. Diamond, A. Fujisawa, M. Yagy, T. Watari, Y. Nagashima and A. Fukuyama, *Plasma Fus. Res.: Rapid Communications* **1**, 037 (2006).
[4] J.R. Robinson, B. Hnat, A. Thyagaraja, K. G. McClements, P. J. Knight, A. Kirk, and MAST Team, *Phys. Plasmas* **20**, 052302 (2013).
[5] B. Hnat, N. Walkden and MAST Team, *Plasma* **2**, 168 (2019).
[6] G.D. Conway, C. Troster, B. Scott, K. Hallatschek and ASDEX Upgrade Team, *Plasma Phys. Control. Fusion* **50**, 055009 (2008).
[7] J. C. Hillesheim, W. A. Peebles, T. A. Carter, L. Schmitz, and T. L. Rhodes, *Phys. Plasmas* **19**, 022301 (2012)
[8] D.F. Kong A.D. Liu, T. Lan, C.X. Yu, J. Cheng, Z.Y. Qiu, H.L. Zhao, H.G. Shen, L.W. Yan, J.Q. Dong, M. Xu, K.J. Zhao, X.R. Duan, Y. Liu, R. Chen1, S.B. Zhang, X. Sun, J.L. Xie, H. Li and W.D. Liu, *Nucl. Fusion*, **57**, 044003 (2017).
[9] G.D. Conway, B Scott, J Schirmer, M Reich, A Kendl and ASDEX Upgrade Team, *Plasma Phys. Control. Fusion* **47**, 1165 (2005).
[10] F. Palermo, X. Garbet, and A. Ghizzo, T. Cartier-Michaud, P. Ghendrih, V. Grandgirard, and Y. Sarazin, *Phys. Plasmas* **22**, 042304 (2015).
[11] F. Palermo, X. Garbet, A. Ghizzo, *Europ. Phys. Journal D* **69**, 8 (2015).
[12] A. Ghizzo and F. Palermo, *Phys. Plasmas* **22**, 082303 (2015).
[13] A. Ghizzo and F. Palermo, *Phys. Plasmas* **22**, 082304 (2015).
[14] M. Ramisch, U. Stroth, S. Niedner and B. Scott, *New J. Phys.* **5**, 12 (2003).
[15] G.D. Conway, F. Palermo, I. Novikau, P. Simon, P. Hennequin and ASDEX Upgrade Team, *46th EPS Conf. Plasma Phys. (Milan)* (ECA) **43C** P2.1091 (2019).
[16] F. Palermo, E. Poli, A. Bottino, A. Biancalani, G.D. Conway and B. Scott *Phys. Plasmas* **24** 072503, (2017).
[17] F. Palermo, E. Poli, A. Bottino, A. Ghizzo, *45th EPS Conf. Plasma Phys. (Prague)* (ECA) **42A** P1.1100 (2018).
[18] F. Palermo, E. Poli and A. Bottino, *Phys. Plasmas* **27** 032507, (2020).
[19] E. Poli, F. Palermo, A. Bottino, O.Maj and H. Weber, *Phys. Plasmas* **27**, 082505 (2020).
[20] J. Petykiewicz *Wave Optics* Springer, 1st ed. (1991)
[21] E. Poli, A. Bottino, O. Mai, F. Palermo and H. Weber *Phys. Plasmas* **28** , 112505 (2021).
[22] F. Palermo, A. Biancalani, C. Angioni, F. Zonca, A. Bottino, *Europhys. Letter* **115**, 15001 (2016).
[23] F. Palermo, A. Biancalani, C. Angioni, F. Zonca, A. Bottino, G.D. Conway and E. Poli, *43rd EPS Conf. Plasma Physics*, P1.046 (2016).
[24] A. Fujisawa, *Nucl. Fusion* **49**, 013001 (2009).
[25] G.D. Conway, E. Poli, T. Happel and ASDEX Upgrade Team, *Plasma Fus. Res.* **5**, S2005 (2010).
[26] S. Jolliet, A. Bottino, P. Angelino, R. Hatzky, T. M. Tran, B. F. McMillan, O. Sauter, K. Appert, Y. Idomura, and L. Villard, *Comput. Phys. Commun.* **177**, 409 (2007).

[27] A. Bottino, T. Vernay, B. Scott, S. Brunner, R. Hatzky, S. Jolliet, B. F. McMillan, T. M. Tran and L. Villard, *Plasma Phys. Control. Fusion* **53**, 124027 (2011).
[28] E. Lanti, N. Ohana, N. Tronko, T. Hayward-Schneider, A. Bottino, B. F. McMillan, A. Scheinberg, A. Biancalani, P. Angelino et al. *Comput. Phys. Commun.* **251**, 107072 (2020).
[29] B. Scott and J. Smirnov, *Phys. Plasmas* **17**, 112302 (2010).
[30] T.S. Hahm, W.W. Lee and A. Brizard, *Phys. Fluids* **31**, 1940 (1988).
[31] H. Sugama and T.-H. Watanabe *J. Plasma Phys.* **72**, 825 (2006).
[32] A. I. Smolyakov, M. F. Bashir, A. G. Elfimov, M. Yagi, and N. Miyato, *Plasma Physics Reports* **42**, 407 (2016).
[33] F. Zonca and L. Chen, *Europhys. Letter*, **83**, 35001 (2008).
[34] V.P. Ermakov *Univ. Izv. (Kiev)* **20** 1 (1880).
[35] A.E. Siegman, Laser (University Science Books, Mill Valley, CA) (1986).
[36] J.R. Pierce, *Proc. Natl. Academy of Sciences*, **47**, 1808 (1961).
[37] Z. Gress and S. Cruz y Cruz, *IOP Conf. Series: Journal of Physics: Conf. Series* **839**, 012024 (2017).
[38] S. Choudhary and L.B. Felsen, *Proc. IEEE* **62**, 1530 (1974).
[39] G. V. Pereverzev, *Reviews of Plasma Physics* (Consultants Bureau, New York, London, 1996), Vol. 19.
[40] E. Poli, G. V. Pereverzev, and A. G. Peeters, *Phys. Plasmas* **6**, 5 (1999).
[41] M. Bornatici and O. Maj, *Plasma Phys. Control. Fusion* **45**, 707 (2003).
[42] A. Biancalani, F. Palermo, C. Angioni, A. Bottino, F. Zonca, *Phys. Plasmas* **23**, 112115 (2016).
[43] P. Simon, PhD Thesis, *Univ. Stuttgart* (2017).
[44] G.D.Conway & ASDEX Upgrade Team *Plasma Phys. Control. Fusion* **50**, 085005 (2008)
[45] G.D.Conway, C.Angioni, F.Ryter, P.Sauter, J.Vicinte, and ASDEX Upgrade team, *Phys. rev. Lett.* **106**, 065001 (2011)